The Applied Biology & Chemistry Journal
https://www.theabcjournal.com
Original Research
eISSN: 2582-8789

Characterization of innately decellularised micropattern pseudostem of *Musa balbisiana* – A non-surface functionalized 3D economic biomaterial scaffold

Deepa Narayanan[1*], Sarita G Bhat[1], and Gaurav Baranwal[2]

[1]*Department of Biotechnology, Cochin University of Science and Technology, Ernakulum-682022, Kerala, India.*
[2]*Department of Medical Physiology, College of Medicine, Texas A&M University, 2403(C) Bryan, TX 77807*

Received June 05, 2021
Revised August 25, 2021
Accepted August 30, 2021
Published September 30, 2021

Supplementary data for this article is available online under https://bit.ly/Narayanan_TABCJ-2021-00013_SupplementaryData

Abstract: Banana (*Musa balbisiana*) pseudostem 3D scaffolds have been developed here for primary eukaryotic cell and cell line culture as an economical, sustainable, eco-friendly alternative for surface-functionalized polymeric and plant tissue-based structures. *Musa* pseudostem 3D micro pattern scaffold (MPM-3Ds) developed by freeze-drying followed by ethylene oxide sterilization yielded 5.6ng of DNA per mg of tissue, confirming its extended decellularised state. Thermo gravimetric analysis, contact angle measurement, uniaxial testing, and FTIR determined thermal stability, wettability, tensile strength, and surface functional groups respectively. Micro and macronutrients, sugars, and amino acids that naturally enrich MPM-3Ds were estimated using EDAX, HPLC, and biochemical analysis. The most important finding was, non-surface functionalized MPM-3Ds supported attachment, growth, and differentiation of human mesenchyme stem cells, human primary hepatocytes like cells, primary mouse brain cortical neurons, mouse fibroblast cells, and human pancreatic cancer cells. MPM-3Ds showed *in vivo* biodegradation and biocompatibility in a preliminary analysis in Sprague Dawley rats. These findings illuminate nature's power to nurture cells in the micropattern cradles of MPM-3Ds that can support innovative research in stem cell differentiation, drug and cosmetic testing, and biosensor development leading to advanced biomedical research.

Keywords: 3D micropattern scaffold; banana pseudostem scaffold; economical 3D scaffold; hepatocyte cell spheroids; natural cellulosic 3D scaffold

1. Introduction

Cells were grown *in vitro* on surface-functionalized three-dimensional (3D) micropattern polymeric scaffolds exhibit *in vivo* like gene expression, cell polarization, and intracellular signaling [1, 2]. The 3D micropattern environment enhances cell-cell and cell-matrix interactions and promotes complex nutrient transport dynamics [3, 4]. Applications of 3D scaffolds primarily include stem cell differentiation, organoid development, drug delivery, drug toxicity evaluation, and elucidation of tumor drug resistance mechanisms [5-9]. Furthermore, these are alternatives for animal testing, play a role in developing personalized medicines, and assist in advanced tissue engineering.

The end-users of the 3D scaffold are pharmaceutical and cosmetic industries as well as biomedical researchers [10]. Commercial 3D scaffolds are highly-priced since scaffold development is expensive in terms of the technique, surface functionalization, skilled labor, need for precision instruments, and extended synthesis duration [2, 5, 11, 12]. Thus, developing economic, sustainable, eco-friendly, and efficient 3D micropattern scaffolds to meet the rise in demand and support research and development.

Intending to address these issues, few research groups have recently made a cross-kingdom advance to explore different surface topographies of tissues from the plant kingdom for 3D scaffold development. Biochemically functionalized decellularized apple hypanthium tissue was employed for *in vitro* 3D cell line culture [13]. Fibronectin-coated decellularized spinach leaf was developed as a vascularized 3D scaffold [14]. Here the surface-functionalized scaffold allows the cells to attach, grow, divide, and migrate among biodegradable natural fiber materials that make up the scaffold. These data stand as evidence that plant tissues can be successfully transformed into 3D scaffolds. The delicate nature of the plant tissue, its expensive surface functionalization, and the need for enzymatic or chemical treatment for decellularisation led to the search for alternative plant tissue [13, 14]. Quest for alternatives led us to explore naturally decellularised, sturdy micropattern plant tissues enriched with biomolecules to address these issues. The biomaterial candidature of the outer sheaths of the pseudostem of banana, which forms the plant's structural support, was chosen.

Banana plant (*Musa* sp.) is cultivated widely in Kerala for its edible fruit, but post-harvest generates extensive biomass agro-waste [15-18]. Research and reports on the

Dr. Deepa Narayanan
Department of Biotechnology,
Cochin University of Science and Technology,
Ernakulum – 682022
Kerala, India
E-mail: deepan301281@gmail.com

Citation: Narayanan D, Bhat SG, Baranwal G (2021). Characterization of innately decellularised micropattern pseudostem of *Musa balbisiana* – A non-surface functionalized 3D economic biomaterial scaffold. *T Appl. Biol. Chem. J*; 2(3):76-88. https://doi.org/10.52679/tabcj.2021.0013

physicochemical evaluation and utilization of banana fiber from the pseudostem as a reinforcing material in upholstery, currency, textiles, and packaging exists, but its use as a scaffold in biomedical applications is a novel idea [19-25]. The presence of micro rectangular architecture, porous interconnected septa, nutrient richness, high cellulosic fiber content makes the pseudostem an ideal candidate for a new 3D scaffold development.

The current study unravels the method of developing non-surface functionalized, decellularised, biocompatible banana (*Musa* sp) pseudostem 3D micropattern scaffold (MPM-3Ds). The physical dimensions and biomolecular constitution enhance its cell adhesion properties. The developed scaffold has been given a facelift as a ready-to-use 3D structure by embedding into polystyrene cell culture wares. This product envisions to meet high demands for such 3D substrates in tissue engineering, drug testing, and biosensor development. A fascinating finding was that unlike other plant-derived decellularised surface-functionalized scaffolds, this MPM-3Ds without any surface functionalization supported the attachment and proliferation of primary cells and cell lines. The MPM-3Ds promoted the attachment and proliferation of human mesenchyme stem cells, supported its differentiation and, unravelled the structure and cell to cell association of mouse primary cortical neurons. Apart from primary cells, the MPM-3Ds also promoted the attachment and proliferation of human and mouse cell lines. Throughout the study duration of a maximum of 50 days, the scaffolds remained structurally intact and pliable for microscopic analysis. Furthermore, the scaffold's biodegradation and compatibility were evaluated in a pilot study of 1- 8 weeks in male Sprague Dawley rats (n=3). Thus, an economical, sustainable, eco-friendly and efficient 3D micropatterned scaffold was developed to meet the rise in demand and support research and development [11, 26-28].

2. Materials and Methods

2.1. Sourcing of the MPM-3Ds material, preservation, sterilization and 3D scaffold incorporated polystyrene plate development

The supportive outermost pseudostem sheath of the banana plant selected for preparing the 3D scaffold consists of tightly packed overlapping sheaths of leaves. The scaffold material retrieved from the live plant by excising the outer sheaths trimmed using a sharp scalpel blade exposes the micropatterned niche [29-31]. The details of which are provided in supplementary method section 1.1.

2.2. Determination of the extend of decellularisation of the pseudostem by DNA quantification

Qiagen-DNeasy® Plant Mini Kit [32] was used to extract DNA from the freeze-dried ETO sterilized 1mg banana pseudostem samples. DNA was then quantified using the Nanodrop instrument (Shimadzu Biotech Biospec Nano) at a wavelength of 280nm. The DNA quantified was then compared to the DNA extracted from 1mg each raw banana leaf, raw pseudostem, and the parent offshoot plant [33]. The DNA from the different sources qualitatively estimated by agarose gel electrophoresis and visualized using ethidium bromide under the Gel Doc system (Syngene G: Box).

2.3. Taxonomic identification of the MPM-3D source plant

The method for taxonomic identification is explained in detail in supplementary methods Section 1.2.

2.4. MPM-3Ds Characterisation

2.4.1. Determination of MPM-3D's physical dimension

The dimensions of the MPM-3Ds evaluated using a scanning electron microscope (SEM); JEOLJSM-6490LA to reveal magnified images of the micro patterns and surface topography [34].

2.4.2. Detection of the functional groups present on MPM-3Ds

Experimental method of FTIR is detailed in supplementary methods Section 1.3; subsection 1.3.1

2.4.3. Evaluation of the thermal stability of the MPM-3Ds

The details of evaluation of thermal stability are furnished in supplementary methods section 1.3; subsection 1.3.2

2.4.4. Determination of the mechanical properties of the MPM-3Ds

The tensile strength and maximum force that the scaffold could withstand was measured using a tabletop uniaxial testing machine (SHIMADZU). The scaffolds were tailored into a rectangular shape with dimensions of 40mm length, 1cm width, and an average thickness of 0.5 mm. Triplicate samples with specific dimensions fixed in the clamps of a UTM machine measures the tension of the strip when drawn apart. The load versus extension measured at 5mm/min at various clamp separation determines the force required to break the scaffolds and the extent to which the samples elongate at that breaking point. The firm strip must be aligned vertically and clamped so that the stresses are uniform across the strip's width and parallel to the direction of loading [35].

2.4.5. Contact angle measurement of the MPM-3Ds

Contact angle measurement procedure is detailed in supplementary methods section 1.3.; subsection 1.3.3.

2.5. Estimation of elements and biomolecules in the MPM-3Ds

2.5.1. Estimation of elemental composition

0.5g of the pseudostem, 4mL concentrated nitric acid (Nice chemicals) heated in a test tube followed by 1ml perchloric acid or hydrogen peroxide digested the sample and made up to 50mL with distilled water. The amount of carbon, hydrogen, nitrogen, and sulfur in the acid digested scaffolds were analyzed using CHNS analyzer Elementar Vario EL III. Analysis of the different macro and micronutrients present in the MPM-3Ds done using Scanning Electron

Microscope – EDAX. (Energy Dispersive Analysis X-ray) JEOL 6390 LA/OXFORD XMX N [33, 36].

2.5.2. Analysis of amino acids and total reducing sugar (TRS)

The amino acid in the pseudostem scaffold was estimated using HPLC as per previous literature. The pseudostem samples were treated with dilute sulphuric acid to hydrolyze hemicellulose. The concentration of TRS was determined using the dinitrosalicylic (DNS) acid method [37, 38].

2.6. Cell attachment, proliferation and differentiation studies on the MPM-3Ds

2.6.1. Human mesenchyme stem cells

The human mesenchyme stem cell (Promo Cell, Germany) was maintained and expanded in IMDM supplemented with 20% fetal bovine serum (FBS) in a 5% CO^2 incubator at 37 °C. $2x10^5$ cells seeded in triplicates on the IMDM drenched sterile freeze-dried MPM-3Ds placed in 6 well polystyrene cell culture plates evaluated by scanning electron microscope 2hrs and 48 hrs of study for cell attachment, and by Calcein AM staining after 14 days for biocompatibility.

2.6.2. Evaluation of change in cells' morphology following Human mesenchyme stem cells to Hepatocyte differentiation on the non-functionalized MPM-3Ds.

$2x10^5$ human mesenchymal stem cells were seeded in triplicates on the IMDM drenched freeze-dried and sterilized MPM-3Ds placed in 6 well plates. Reagents used for differentiation was procured from Sigma Aldrich. The cells were serum-deprived for two days in IMDM supplemented with 20ng/mL EGF (Epidermal growth factor) and 10ng/mL bFGF (Fibroblast growth factor-basic human). The media then replaced with IMDM enriched with 20ng/mL H.G.F. (Hepatocyte growth factor human),10ng/mL bFGF, and nicotinamide 0.61g/L and continued for seven days. After that, IMDM with 20ng/mL OSM (Oncostatin M human) and one µm/L dexamethasone and 50mg/L, ITS premix was added to cells and continued for 50 days on MPM 3Ds. The scaffolds were then processed for SEM for morphological analysis, calcein staining for live cell imaging, and confocal imaging of differentiation-specific markers. Immunofluorescence assay for detecting human hepatocyte-like cell-specific markers (Invitrogen) OCHIE5 and Cytochrome P 450 was performed by washing the scaffold twice in cold PBS and fixing in 4% paraformaldehyde for 20 minutes at 4 °C. The blocking solution used was 2% BSA Cells were incubated overnight at 4 ° C with an antihuman monoclonal antibody against OCHIE5 and Cytochrome P450 (cyp2b6). Cells were washed and incubated at room temperature for 50 minutes with FITC-conjugated anti-mouse/anti-rabbit secondary antibodies-Invitrogen (1:2000 dilution) [39-41].

2.6.3. Mouse primary cortical neurons

Mouse cortical primary neurons were isolated from the brain of pup (postnatal day-1) and seeded on the scaffold directly to visualize the preliminary attachment of the cells (IAEC -363/GO/Re/S/05/CPCSEA,28/12/2017). The cells were maintained in the Neurobasal-A supplemented with B27 and L-glutamine (media and supplements from Gibco) for 14 days. After incubation, the scaffold's triplicate sets were analyzed for cell attachment, cell morphology, and scaffold interaction by SEM imaging.

2.6.4. Human pancreatic cancer cell line and Mouse fibroblast cell lines

The details of cell culture on scaffolds are provided in supplementary methods section 1.4.; subsection 1.4.1

2.7. Scaffold processing for imaging

Scaffold processing details is provided in supplementary methods section 1.5.

2.8. Preliminary in vivo evaluation of biocompatibility and biodegradation in Sprague Dawley rats

The institutional ethics committee approved a pilot study on in *vivo* biocompatibility and biodegradation of MPM-3Ds by subcutaneous implantation in male Sprague Dawley rats (n=3) (IAEC 363/GO/Re/S/01/CPCSEA,28/12/2017). The rats were anesthetized using intramuscular injection of 35.0 mg/kg ketamine and 5.0 mg/kg xylazine in the gluteal area (3K:2X,0.04-0.05mL/250 g rat). A surgical incision was made on the dorsal right side of the animal, and MPM-3Ds were placed and sutured using commercially available vicryl. Sham-operated and un-operated rats were kept as controls. The animals were euthanized after one week, four weeks, and eight weeks using carbon dioxide chamber. Cardiac puncture and blood draw was done for CRP and analysis of polymorphs. The subcutaneous tissue and implant were retrieved for histopathological evaluation to visualize angiogenesis, biodegradation, and biocompatibility.

2.9. Statistical Analysis

All presented values are the average ± standard deviation. Statistical analyses involved mixed-design ANOVA followed by Tukey's comparison.

3. Results

3.1. Sourcing of the MPM-3Ds material, preservation, sterilization and 3D scaffold incorporated polystyrene plate development

The detailed results are furnished in the supplementary results section 2.1 (Suppl. Figure S1).

3.2. Determination of the extend of decellularization of the pseudostem

The DNA content per mg of tissue from freeze-dried and ETO sterilized pseudostem was 5.6ng, which is only about 10 % of 55.29ng DNA derived from the parent plants leaf. Hence reveals an extended decellularised nature (90%) of the pseudostem [42, 43]. A faint band in agarose gel corresponding to the DNA load in freeze-dried and raw

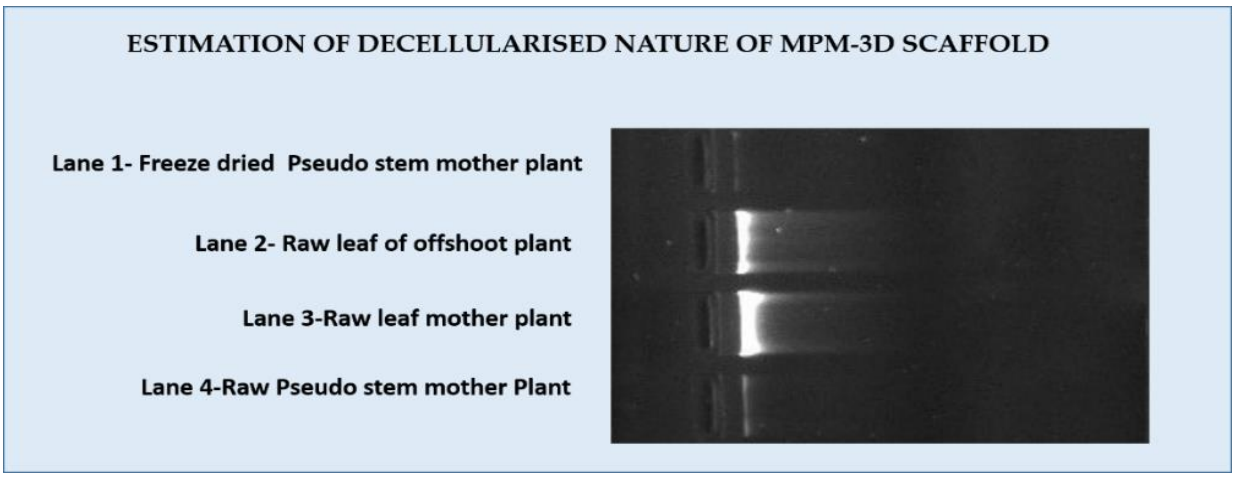

Figure 1: The figure shows the DNA band visualized on the agarose gel from the leaf of the banana mother plant, the offshoot plant form prominent bands when compared to the raw and freeze-dried pseudostem.

pseudostem (**figure 1; lane 1 and 4**), when compared to the significant bands corresponding to the DNA isolated from leaf of the offshoot plant and mother plant (**figure 1; lane 2 and 3**), substantiates our DNA quantification data.

3.*3. Taxonomic identification of the MPM-3D source plant*

The results are furnished in the supplementary results section 2.2 (Suppl. Figure S2, S3).

3.4 MPM-3Ds Characterization

3.4.1. Determination of the physical dimensions of MPM-3D

The scanning electron microscope images and photographic images of freeze-dried MPM-3Ds revealed a micro rectangular cavity (0.5mm X 1mm X 0.5mm) with interconnecting porous septa (0.05mm diameter) arranged in a series resting on a sturdy base (**Figure 2 - A, C**).

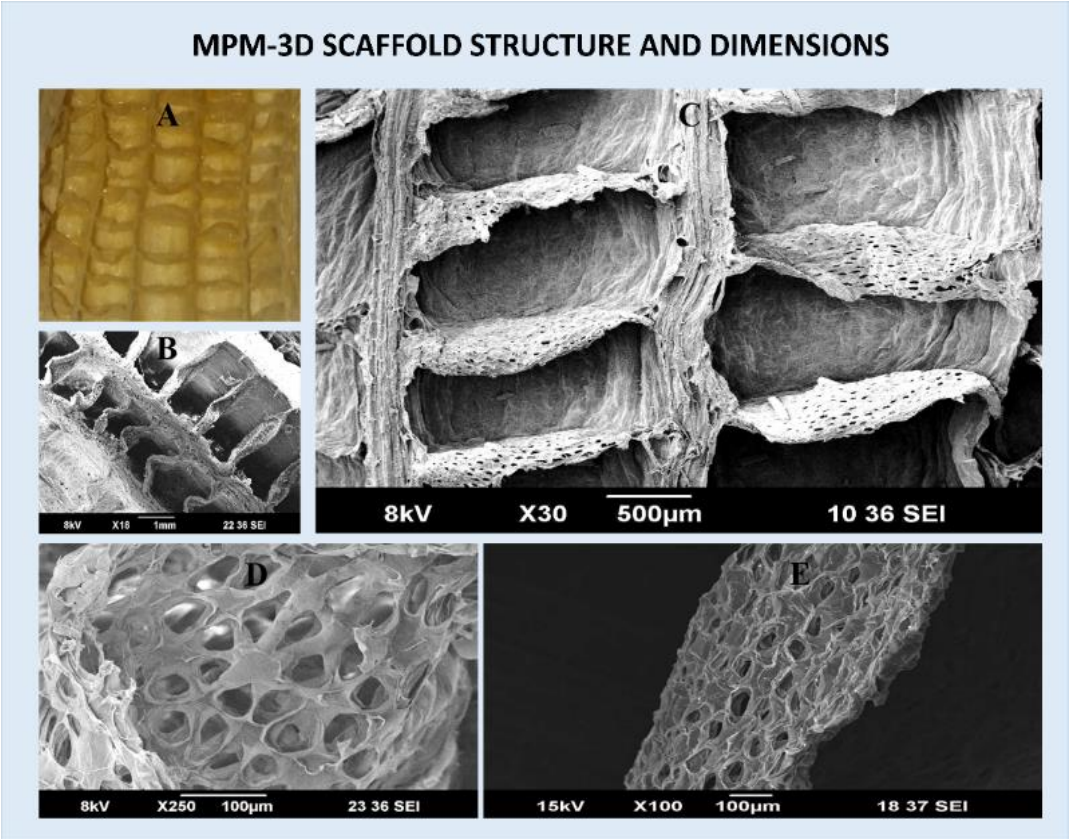

Figure 2: (A) Photograph of the banana pseudostem scaffold with the micro pattern rectangular sockets; (B) the MPM-3D scaffold after 50 days in media showing scaffold integrity; (C) SEM image of the micro patterns evident on the banana pseudostem scaffold; (D and E) SEM image of the interconnecting septa present between the micro rectangular cavities of the MPM-3Ds.

Citation: Narayanan D, Bhat SG, Baranwal G (2021). Characterization of innately decellularised micropattern pseudostem of *Musa balbisiana* – A non-surface functionalized 3D economic biomaterial scaffold. *T Appl. Biol. Chem. J;* 2(3):76-88. https://doi.org/10.52679/tabcj.2021.0013

Figure 2 - D, E) shows magnified images of interconnecting septa between micro rectangular cavities of scaffold. The MPM-3Ds are seen to retain morphology even 50 days after remaining in cell culture media, as seen in **figure 2 - B**.

3.4.2. Detection of the functional groups present on MPM-3Ds

FTIR results are detailed in supplementary results section 2.3.3 (Suppl. Figure S4).

3.4.3. Evaluation of the thermal stability of the MPM-3Ds

The details of the thermal stability of MPM-3DS are given under supplementary results section 2.3.2 (Suppl. Figure S5).

3.4.4. Determination of the mechanical properties of the MPM-3Ds

The maximum force (Fmax) which 1mm thick and 12mm wide MPM-3Ds piece can bear while testing once the yield point has crossed for scaffold material is 228.2 ± 22.75 N. The elongation of scaffold at this F max is 2.04 ± 0.22% of original length which shows that the scaffold is non-elastic. The tensile strength of the MPM-3Dscaffold is 20.5 ± 2.42 MPa.

3.4.5. Contact angle measurement of the MPM-3Ds

The details are provided under supplementary results section 2.3.3

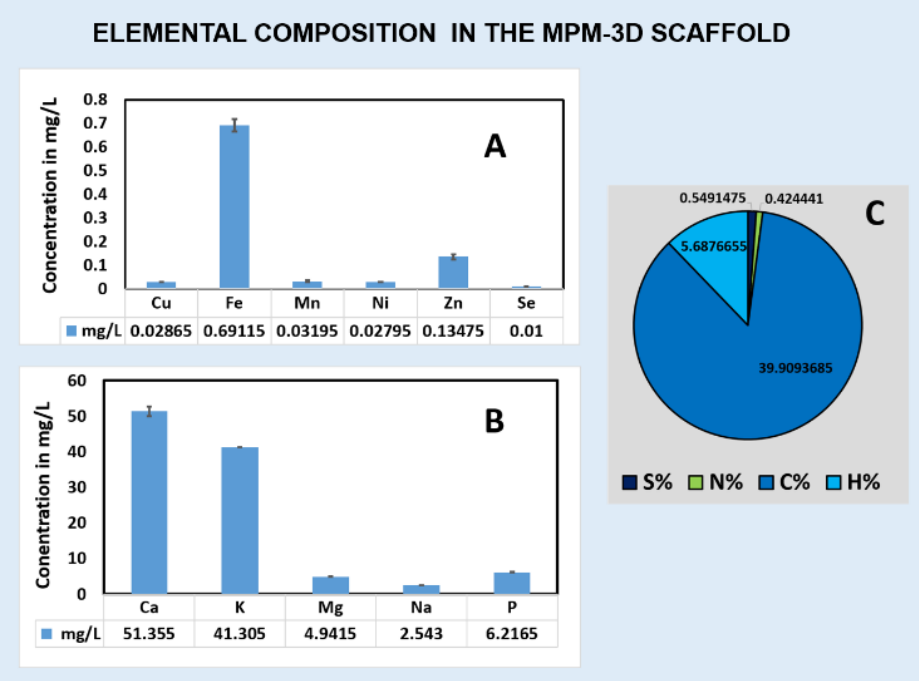

Figure 3: The graphs represent the elemental composition of MPM-3Ds material. (A) The graph shows the mg/L concentration of micronutrients in the sample; the (B) graph shows the mg/L concentration of macronutrient; (C) graph represents the mass fraction weight percentage of CHNS content in the MPM-3Ds material.

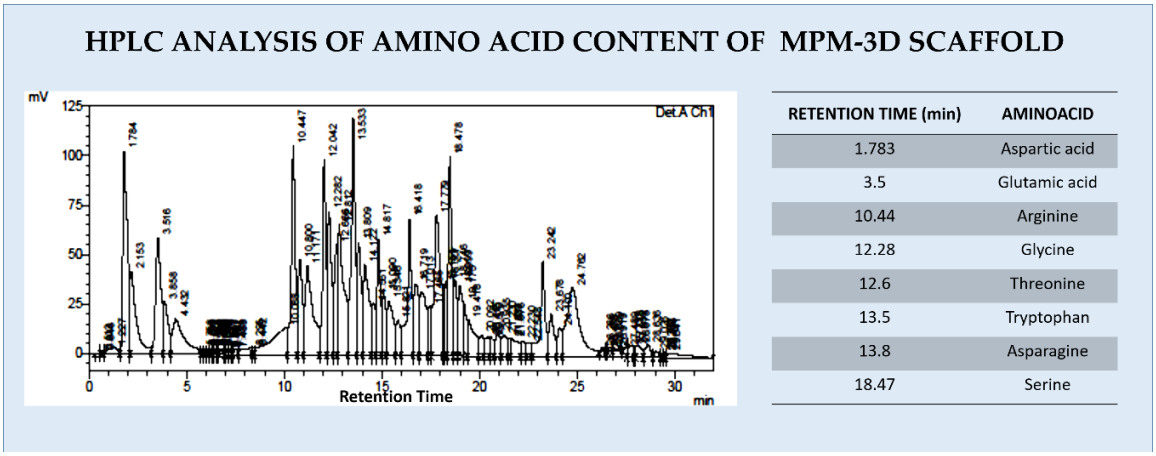

RETENTION TIME (min)	AMINOACID
1.783	Aspartic acid
3.5	Glutamic acid
10.44	Arginine
12.28	Glycine
12.6	Threonine
13.5	Tryptophan
13.8	Asparagine
18.47	Serine

Figure 4: The figure shows the chromatogram of the HPLC analysis of the amino acid content in the MPM-3Ds the list of amino acid corresponding to the major peaks obtained in the chromatogram.

Citation: Narayanan D, Bhat SG, Baranwal G (2021). Characterization of innately decellularised micropattern pseudostem of *Musa balbisiana* – A non-surface functionalized 3D economic biomaterial scaffold. *T Appl. Biol. Chem. J*; 2(3):76-88. https://doi.org/10.52679/tabcj.2021.0013

3.5. Estimation of elemental composition and biomolecules in the MPM-3Ds

3.5.1. Estimation of elemental composition, macro, and micronutrients

The SEM EDAX analysis of the MPM-3Ds shows presence of micronutrients such as copper, iron, manganese, nickel, zinc, selenium (**figure 3-A**). The concentration of iron was 0.69 mg/L and stood highest in concentration compared to rest of the micronutrients. The macronutrients detected at the highest concentrations were 51.35 mg/L calcium and 41.3 mg/L potassium, followed by phosphorous magnesium and sodium, as represented in **figure 3-B**. The CHNS analysis reveals mass fraction weight expressed in percentage. **Figure 3-C** reshows that 39.9 % of the sample is carbon, 5% hydrogen, 0.54% nitrogen and 0.42% sulfur.

3.5.2. Analysis of amino acids and total reducing sugar (TRS)

The chromatogram and corresponding list in **figure 4** represent the amino acids detected by HPLC in the MPM-3Ds material. The scaffold is rich in different amino acids such as arginine (R), glycine (G), aspartic acid (D), etc. Acid hydrolysis was performed for the detection of carbohydrates and 0.62m/mL glucose and 0.27mg/mL mannose was detected in the MPM-3Ds material.

3.6. Biocompatibility, cell attachment, and proliferation

The different cells seeded on the scaffolds have exhibited good attachment and proliferation as elaborated below:

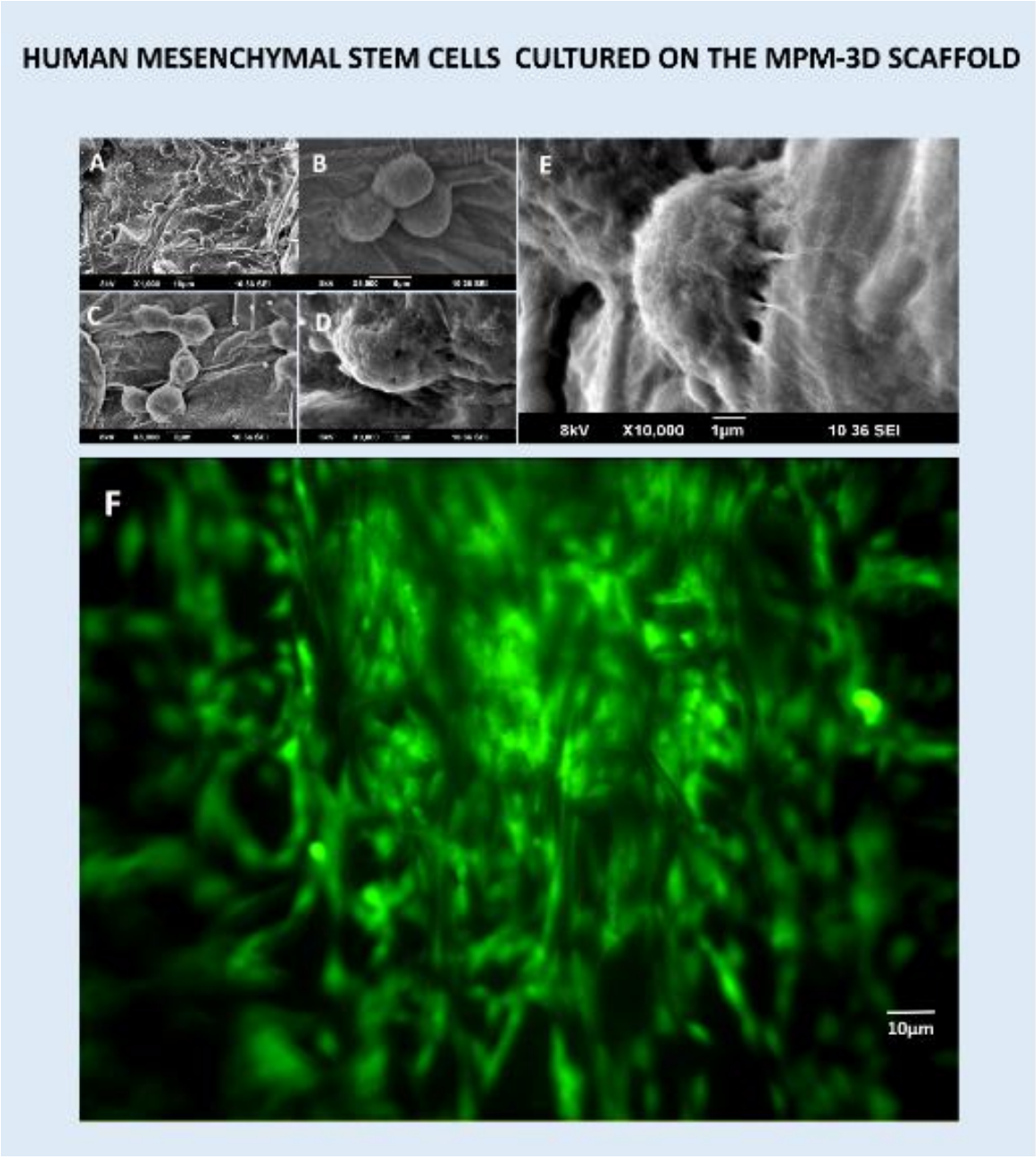

Figure 5: (A-E) are the SEM images of the hMSC cultured on the MPM-3Ds and (F) is the calcein stained hMSC on the scaffold on day 14.

Citation: Narayanan D, Bhat SG, Baranwal G (2021). Characterization of innately decellularised micropattern pseudostem of *Musa balbisiana* – A non-surface functionalized 3D economic biomaterial scaffold. *T Appl. Biol. Chem. J;* 2(3):76-88. https://doi.org/10.52679/tabcj.2021.0013

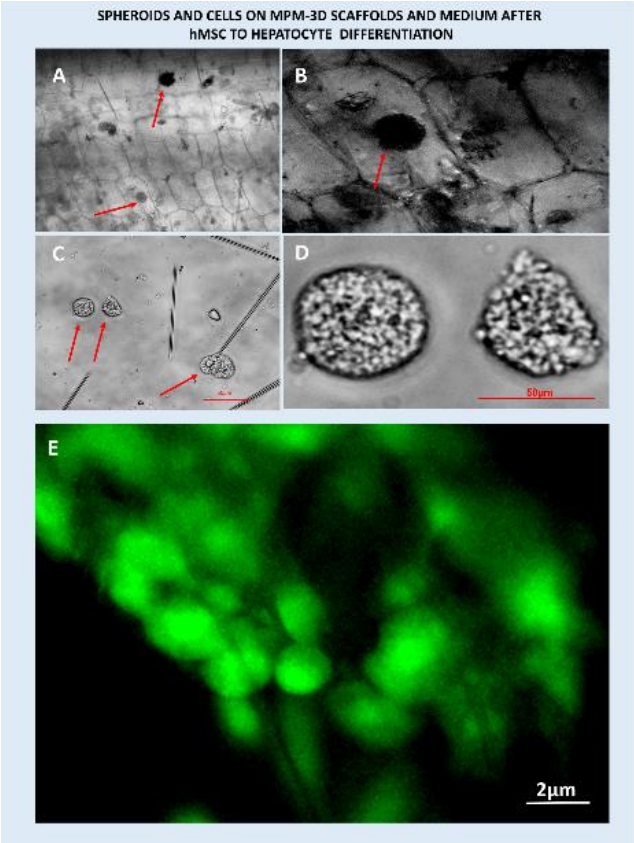

Figure 6: (A and B) show the light microscope images of the spheroids formed within the MPM -3D scaffold after the hMSC differentiation treatment, (C and D) show the spheroids that were released into the medium from the MPM-3Ds, and (E) is the calcein stained image of the cells on the scaffold after differentiation**.**

3.6.1. Human mesenchymal stem cells

Human mesenchymal stem cells attached and proliferated well on the scaffold. The cells have extended their periphery and are intricately attached to the scaffold. **Figure 5 A-E** shows the hMSC attached to scaffold on day two and **figure 5-F** shows calcein-AM live stained cells throughout the scaffold after 14 days of seeding. The topography of the MPM-3Ds favors the 3D attachment and proliferation of the cells.

3.6.2. Evaluation of change in morphology of cells following Human mesenchyme stem cells to Hepatocyte differentiation on the non-functionalized MPM- 3Ds

The human mesenchymal stem cells were subjected to hepatocyte differentiation protocol for 20 days and further maintained for another 30 days for spheroid formation. Post differentiation, the scaffolds' bright-field microscopic images showed opaque spherical outlines, and 50µm spheroid spillage into the cell culture medium was observed as shown in **figure 6**.

The surface of the MPM-3D was then scanned and, SEM images of the scaffold revealed the presence of a massive number of proliferated primary human hepatocyte-like cells with numerous bud-like projections on the surface resembling a berry-like morphology and a central invagination (**figure 7**). The different stages of formation of spheroids where the cells are seen to migrate into a cluster on the scaffolds can be observed as well.

The preliminary evaluation for the presence of cell surface markers OCHIE5 and Cytochrome P450 (cyp2b6) was

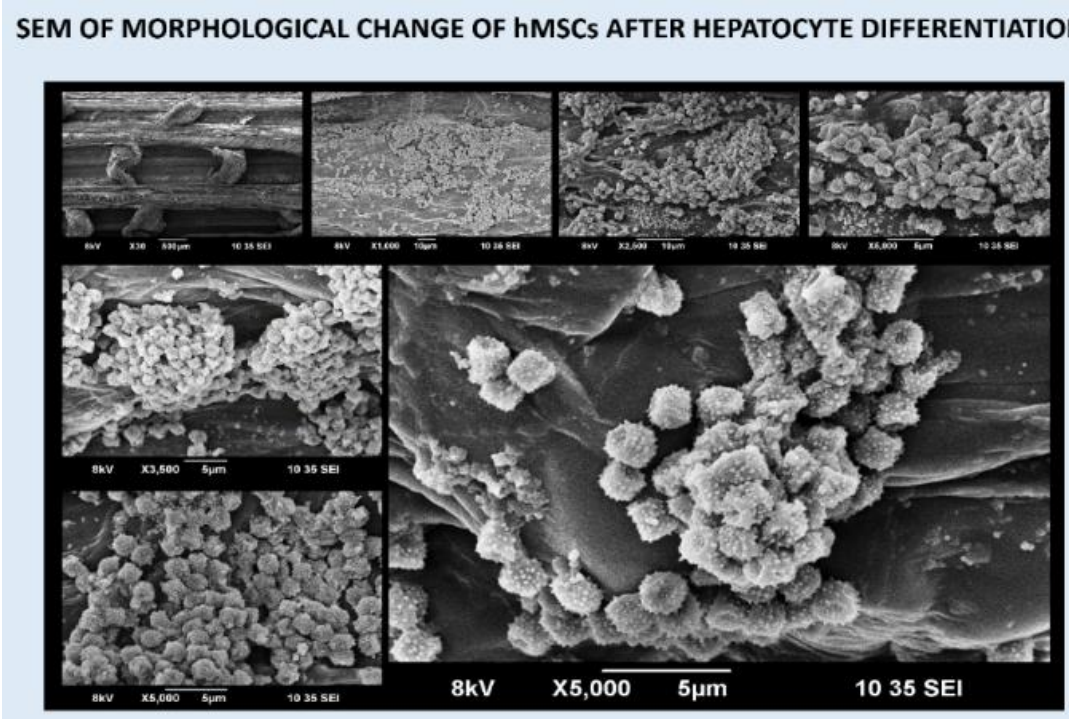

Figure 7. All the panels depict the different SEM magnification images of the MPM-3Ds bearing cells after hMSC to hepatocyte differentiation. The cells seen here are in the process of aggregating into spheroids.

Citation: Narayanan D, Bhat SG, Baranwal G (2021). Characterization of innately decellularised micropattern pseudostem of *Musa balbisiana* – A non-surface functionalized 3D economic biomaterial scaffold. *T Appl. Biol. Chem. J;* 2(3):76-88. https://doi.org/10.52679/tabcj.2021.0013

positive, as observed under confocal microscope (**figure 8**) [39, 44].

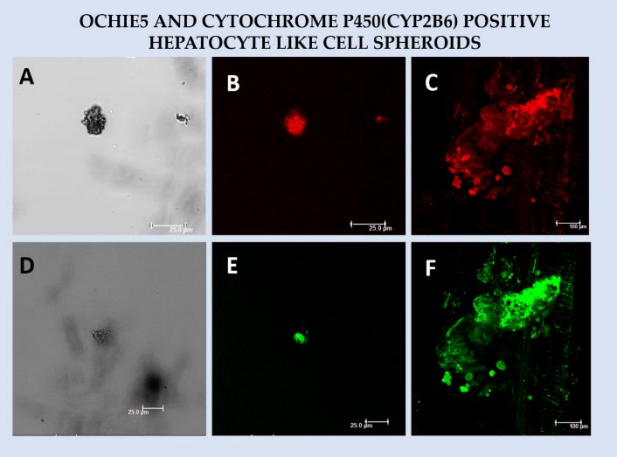

Figure 8: (A and D) are the bright-field images of a spheroid and OCHIE5 positive red fluorescence emitting; (B) single spheroid; (C) spheroid cluster in the scaffold depth. Cyp2b6 positive green fluorescence emitting; (E) single spheroid and (F) spheroid cluster in the scaffold depth.

3.6.3. Mouse primary cortical neurons

Mouse primary cortical neuron cells isolated from the brain of mouse pups were attached to MPM-3Ds despite the absence of any surface modifications. The spreading of cells on scaffold is visible in SEM analysis and a typical neuronal structure unfolding could also be observed as represented in **figure 9**.

3.7. Preliminary in vivo evaluation of biocompatibility and biodegradation in Sprague Dawley

The biomaterials subcutaneously implanted were found to be biocompatible, and biodegradation occurred after one week as observed in histopathology of samples at 1-, 4- and 8-week post-subcutaneous implantation. The histopathological images after one week of subcutaneous implantation of scaffold show intraepidermal neutrophilic infiltrate papillary dermis inflammatory infiltrate of histiocytes and neutrophils along with plump fibroblasts. The reticular dermis, subcutis, and skeletal muscle layer disrupted by dense inflammation and fibrosis surrounded implanted material. Edematous granulation of tissue was observed both at the surroundings and extending into the material (**figure 10**).

The granulation tissue is composed of plump spindle-shaped fibroblasts; numerous variably sized, predominantly thin-walled ectatic capillaries lined by plump endothelial cells; and dense inflammatory infiltrate composed predominantly of neutrophils. Also seen are histiocytes and multinucleate giant cells with ingested implant material. Most of the implant material is replaced by inflammation and necrotic debris. The adjacent papillary dermis also shows dermal appendages and ectatic vessels. After four weeks post-implantation, sections from the skin show lining normal corrugated epidermis overlying dermis with dermal appendages and ectatic vessels. At the site of the previous implant, the epidermis is flattened. The dermis underlying flattened epidermis show inflammation and minimal fibrosis extending through dermis and subcutis focally replacing the skeletal muscle layer. The inflammation is composed predominantly of histiocytes along with mast

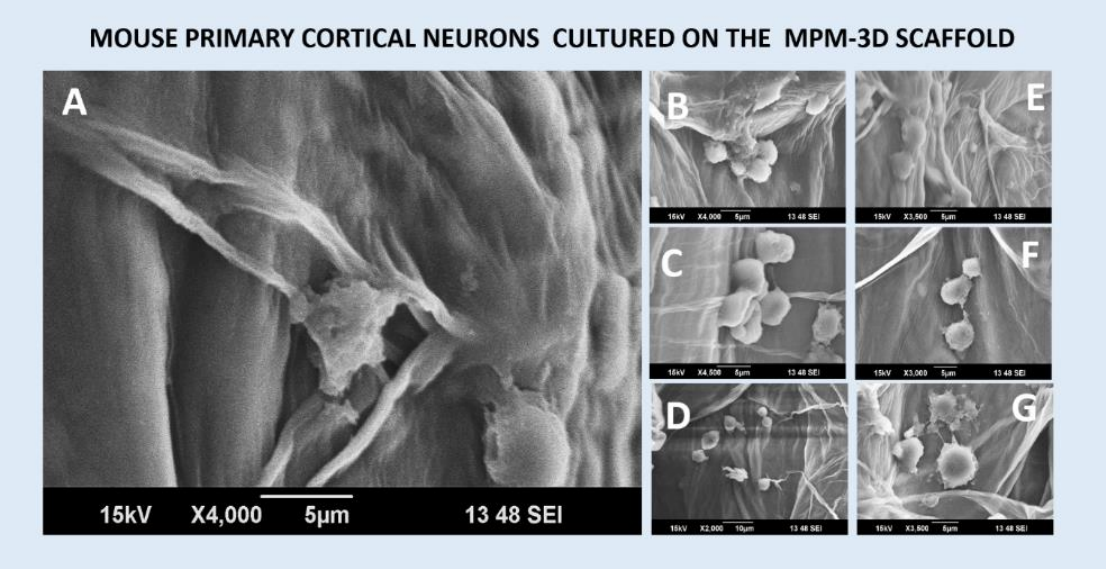

Figure 9: The images (A–E) show the different SEM magnification images of mouse cortical neurons on day 14 on the MPM-3Ds.

3.6.4. Human pancreatic cancer cell line and Mouse fibroblast cell lines

Supplementary results section 2.4.1 details the observation of cell growth and proliferation on MPM-3D scaffolds (Suppl. Figure S6 and S7).

cells, multinucleate giant cells with ingested refractile foreign body material, and hemosiderin-laden macrophages. An epidermal inclusion cyst was also noted at the same site.

ANOVA revealed a significant interaction effect of treatment and duration on the % polymorphs in blood [F

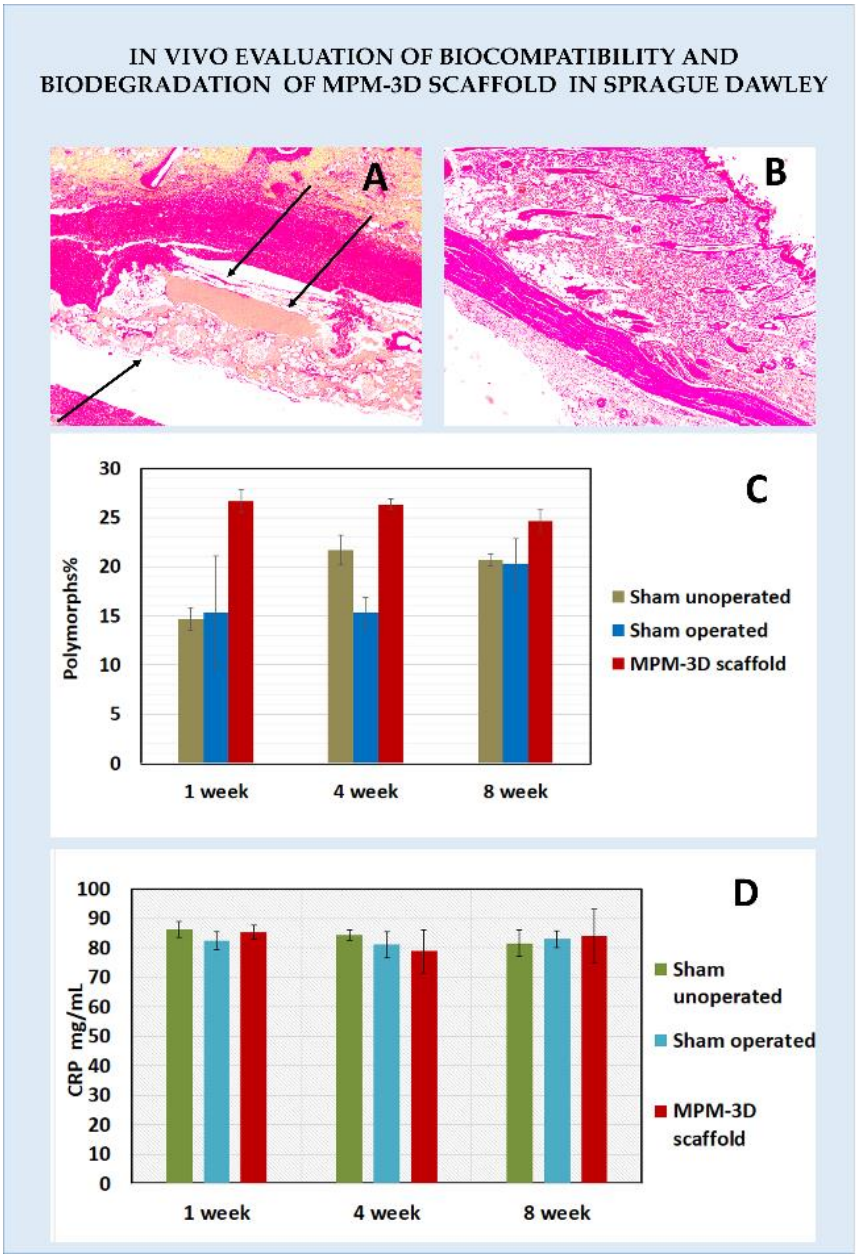

Figure 10: (A and B) are the H and E stained bright-field images of the subcutaneously implanted MPM-3Ds in male Sprague Dawley rats after one week and four weeks, respectively. The arrows in image (A) point out the MPM-3Ds in the underlying region of the skin after one week of implantation. (C) the graph represents the percentage of polymorph increase in the blood, and (D) is the graphical representation of the C-reactive proteins in mg/mL in the blood of the animal post-implantation when compared to sham-operated and unoperated.

(2.93, 8.78) = 29.31, p = < 0.001, η^2 = 0.831]. Follow-up tests showed a significant increase in MPM-3Ds ($p < 0.0001$) compared to sham operated and sham unoperated groups in the 1st week. Polymorphs % was significantly increased in MPM-3Ds and sham unoperated ($p < 0.0001$) compared to sham operated in the 4th week. There was a considerable increase in polymorphs % in sham unoperated group during the 4th week which yielded a statistically non-significant ($p > 0.05$) outcome compared to MPM-3D. However, this increase was later found to be decelerated during the 8th week with a significantly lower polymorphs % for both sham unoperated ($p < 0.05$) and sham operated ($p < 0.01$) groups compared to MPM-3Ds. The evaluation of CRP showed no significant effect of MPM-3D implantation [F (2, 6) = 0.17, p = > 0.05, η^2 = 0.03] or duration of implant [F (1.64, 9.83) = 2.41, p = > 0.05, η^2 = 0.1], on CRP [45]. The histopathological analysis of the one-week implant reveals the presence of these polymorphs at the site of the implant that phagocytosed the material and removed it completely by week four.

4. Discussion

Cells grown on 3D scaffolds are an accurate representation of cells homed within the organs *in vivo*; thus, pharmaceutical, cosmetic, and biomedical research groups depend on 3D sensitive cell-based assays to bypass exhaustive animal testing. 3D micropattern scaffold

demands long hours of skilled labor and precision instruments for its development, followed by detailed micropatterning and expensive surface functionalization. Procurement of these scaffolds usually exceeds the funds allotted for basic research, which is a prime reason for slow or gradual transition from 2D to 3D culture systems [10]. Among the different materials evaluated for economic 3D scaffold synthesis, plant tissues are the most sustainable and eco-friendly choice for 3D scaffolding. However, the loss of scaffold due to delicate nature of the plant tissue, adds to the need for surface functionalization, and decellularisation with chemicals or enzymes which are the areas that demand economic alternatives. Hence, we selected naturally decellularised banana pseudostem and tailored it to expose micropattern and developed it as a 3D scaffold. This non-surface functionalized MPM-3Ds successfully homed mammalian primary cells, cancer cell lines, and supported hepatocyte differentiation. The scaffold was observed to be biocompatible in Sprague Dawley rats in a 1–8-week pilot study. MPM-3Ds embedded in polystyrene well plates developed in this study is an economical, sustainable, and eco-friendly choice to assist research and development.

Musa balbisiana located in Vypin island, Kerala (10°02' 48.1" N 76°13' 33.6"E) was the source for the outer sheath of pseudostem used for the MPM-3Ds development. The DNA content of the freeze-dried scaffold was 5-6.5 ng of DNA/ mg of plant tissue, which was 89-90% decellularised when compared to DNA extracted from 1mg leaf (55.27 ng) [43]. Hence enzyme or detergent-based decellularisation was omitted in this scaffold synthesis. Ethylene oxide gas had deep scaffold penetration, and the MPM-3Ds embedded polystyrene well plates were packed in the sterilized material-storage indicator packs until use. Polystyrene wells supported hassle-free scaffold handling, media change, assays and processing for microscopic imaging. The scaffold remained intact at all endpoints of *in vitro* experiments except the interconnecting septa, which had lost its rigidity and appeared relaxed. Debris consisting of calcium oxalate crystals and few microfibers was observed in the wells. Thus, the scaffold's physical dimensions and the surface topography are suitable for long-term cell culture, and the facelift has given by merging the MPM-3Ds into a polystyrene well plate makes it a ready-to-use convenient cell culture commodity.

3D scaffolds are often coated with galactose, laminin, collagen, and other biomolecules to initiate cell attachment [14, 46]. The MPM-3D scaffolds devoid of surface functionalization were innately rich in biomolecules favoring cell growth. The scaffold favored the attachment and proliferation of hMSC, L929, MIA-Pa-Ca-2, mouse brain cortical neurons, as well as the differentiation and migration of hepatocyte-like cell spheroids. The scaffolds SEM EDAX data revealed high levels of iron, which is known to promote cell proliferation and differentiation and calcium; via cytoskeleton interaction, it has proved to assist the movement of cells and its growth [36, 47-49]. Among the amino acids detected by HPLC were arginine (R), glycine (G) aspartic acid (D), probably assembled as RGD sequence in proteins to promote the cell adhesion with glucose and mannose as sources of energy. The IR spectrum of the MPM-3Ds was indicative of cellulose, pectin, and lignin [50-52]. These biopolymers form the walls, floor, and interconnecting septa in a pattern that imparts porosity yet maintains sturdiness. The hydrophilic scaffolds imbibed culture medium, keeping the attached cells well-nourished and cleared metabolic byproducts efficiently. hMSC differentiated to hepatocyte-like cell spheroids with raspberry-like cell morphology having a central invagination and small podia like extensions on the surface [41, 52]. SEM images revealed the migration of these cells at different stages of spheroid formation. They were stained positive for Hep par 1 (OCHIE5), a carbamoyl phosphate synthase 1 enzyme involved in urea synthesis, and cytochrome P450, which stands evidence for metabolic activity and substantiate differentiation [39, 44].

A pilot study on the subcutaneous implantation of scaffolds in male Sprague Dawley rats (n=3) proved its *in vivo* biocompatibility and biodegradability. Moderate localized edema post-implantation subsided within 12-24 hrs, meanwhile regaining regular activity and food and water intake within the first 4-6 hrs. Keeping the animals in pairs reduced stress and improved mutual grooming and overall well-being, which could have helped post-operative recovery. After one week of implantation, the histology of the tissue samples showed intraepidermal neutrophilic infiltrates, inflammatory infiltrates of histiocytes, and fibroblasts around the scaffold. Multinucleate giant cells with ingested implant material were also prominent. After four weeks post-implantation, the epidermis at that site flattened, and the scaffold, no longer traced at the implant site. However, no significant variation in the C-reactive protein between the sham-operated and biomaterial implanted rat group. Levels of polymorphs that are the cells involved in phagocytosis of the material were elevated in the MPM-3Ds inserted group throughout the eight weeks of study. Future research on the immune response of small animal models towards autologous cell-seeded MPM-3Ds will add depth and dimensions to our current understanding.

This study has highlighted the MPM-3Ds primary cell, cell line, and differentiation support potential without the need for surface functionalization. The scaffold was not subject to decellularisation and had an extended in vitro integrity, which proves that our selection of the biomaterial candidature of the pseudostem of bananas indeed the best choice of plant tissue for 3D scaffold development. The study has its limitations and requires detailed research on the molecular expressions of differentiated cells with histological evaluation of the *in vitro* spheroids and a detailed evaluation of its metabolic pathways. Experimental design and implementation for differentiation of hMSC to other cell lineages will add luster to the valuable results obtained here. The physical features of the MPM-3Ds such as its thermal stability up to 100°C and tensile strength of 20.5 ± 2.42MPa with the ability to withstand 228.2 ± 22.75 N force opens up future research on MPM-3Ds and polymer/ceramic/metal-based fusion scaffolding. The development of MPM-3Ds embedded polystyrene cell culture commodity and the critical findings in this study is at the crossroad of immense possibilities for 3D scaffold-based biomedical research and product development.

Citation: Narayanan D, Bhat SG, Baranwal G (2021). Characterization of innately decellularised micropattern pseudostem of *Musa balbisiana* – A non-surface functionalized 3D economic biomaterial scaffold. *T Appl. Biol. Chem. J;* 2(3):76-88. https://doi.org/10.52679/tabcj.2021.0013

Declarations

Patent: Provisional patent application number TEMP/E-1/58889/2020-CHE

Acknowledgements: Dr. Syamkumar for statistical advice, Centre for Neuroscience CUSAT for donating the mouse cortical neuronal cells

Author Contribution: First author: DN-project proposal, submission to funding source, finance management, performing experiments, data collection, writing manuscript, editing; second author: SGB-providing infrastructure and guidance for the accomplishment of the project, editing of manuscript; third author: GB-experimental contribution, data compiling and manuscript proofreading.

Funding: This research was funded by UGC DSK postdoctoral fellowship, India, Grant number: F.4-2/2006(BSR)/BL/16-17/0048

Conflict of Interest: "The authors have no conflict of interest." "The funders had no role in the design of the study; in the collection, analyses, or interpretation of data; in the writing of the manuscript, or in the decision to publish the results".

References

[1] Li CY, Stevens KR, Schwartz RE, Alejandro BS, Huang JH, Bhatia SN (2014). Micropatterned cell-cell interactions enable functional encapsulation of primary hepatocytes in hydrogel microtissues. *Tissue Eng Part A*; 20(15-16):2200-12. [CrossRef] [PubMed]

[2] Sarkar S, Lee GY, Wong JY, Desai TA (2006). Development and characterization of a porous micro-patterned scaffold for vascular tissue engineering applications. *Biomaterials*; 27(27):4775-82. [CrossRef] [PubMed]

[3] Khoruzhenko AI (2011). 2D- and 3D-cell culture. *Biopolym Cell*; 27(1):17-24. [CrossRef]

[4] Edmondson R, Broglie JJ, Adcock AF, Yang L (2014). Three-Dimensional Cell Culture Systems and Their Applications in Drug Discovery and Cell-Based Biosensors. *Assay Drug Dev Technol*; 12(4):207-18. [CrossRef] [PubMed]

[5] Park HJ, Lee OJ, Lee MC, Moon BM, Ju HW, *et al* (2015). Fabrication of 3D porous silk scaffolds by particulate (salt/sucrose) leaching for bone tissue reconstruction. *Int J Biol Macromol*; 78:215-23. [CrossRef] [PubMed]

[6] Deglincerti A, Etoc F, Guerra MC, Martyn I, Metzger J, Ruzo A, *et al* (2016). Self-organization of human embryonic stem cells on micropatterns. *Nat Protoc*; 11(11):2223-2232. [CrossRef] [PubMed]

[7] Benton G, Arnaoutova I, George J, Kleinman HK, Koblinski J (2014). Matrigel: from discovery and ECM mimicry to assays and models for cancer research. *Adv Drug Deliv Rev*; 79-80:3–18. [CrossRef] [PubMed]

[8] Brown JM, Giaccia AJ (1998). The unique physiology of solid tumors: opportunities (and problems) for cancer therapy. *Cancer Res*; 58(7):1408–16. [PubMed]

[9] Pan T, Song W, Cao X, Wang Y (2016). 3D Bioplotting of Gelatin/Alginate Scaffolds for Tissue Engineering: Influence of Crosslinking Degree and Pore Architecture on Physicochemical Properties. *J Mater Sci Technol*; 32(9):889-900. [CrossRef]

[10] Markets and Markets (2019). 3D Cell Culture Market by Product (Hydrogel, Hanging Drop, Bioreactor, Microfluidics, Magnetic Levitation), Application (Cancer, Stem Cell, Toxicology, Tissue Engineering), End User (Pharmaceutical, Biotech, Cosmetics), Region - Global Forecast to 2024. https://www.marketsandmarkets.com/Market-Reports/3d-cell-culture-market-191072847.html. (accessed on September 12, 2019).

[11] Srivastava RK (2017). Electrospinning of patterned and 3D nanofibers. In: *Electrospun Nanofibers*. Woodhead Publishing, India. [CrossRef]

[12] Chung TW, Yang J, Akaike T, Cho KY, Nah JW, *et al* (2002). Preparation of alginate/galactosylated chitosan scaffold for hepatocyte attachment. *Biomaterials*; 23(14):2827–34. [CrossRef] [PubMed]

[13] Modulevsky DJ, Lefebvre C, Haase K, Al-Rekabi Z, Pelling AE (2014). Apple derived cellulose scaffolds for 3D mammalian cell culture. *PLoS One*; 9(5):e97835. [CrossRef] [PubMed]

[14] Robbins ER, Pins GD, Laflamme MA, Gaudette GR (2020). Creation of a contractile biomaterial from a decellularized spinach leaf without ECM protein coating: An in vitro study. *J Biomed Mater Res A*; 108(10):2123-2132. [CrossRef] [PubMed]

[15] Phirke NV, Patil RP, Chincholkar SB, Kothari RM (2001). Recycling of banana pseudostem waste for economical production of quality banana. *Resour Conserv Recycl*; 31(4):347–53. [CrossRef]

[16] Mukundan S, Narayanankutty A (2017). Traditional Fruits of Kerala: Bioactive Compounds and their Curative Potential in Chronic Diseases. *Curr Nutr Food Sci*; 13(4):279-289. [CrossRef]

[17] Kumar BM (2005). Land use in Kerala: changing scenarios and shifting paradigms. *J Trop Agric*; 43(1-2):1-12.

[18] Rajasekharan P, Veeraputhran S (2002). Adoption of intercropping in rubber smallholdings in Kerala, India: A Tobit analysis. *Agrofor Syst*; 56:1-11. [CrossRef]

[19] Joseph S, Sreekala MS, Oommen Z, Koshy P, Thomas S (2002). A comparison of the mechanical properties of phenol formaldehyde composites reinforced with banana fibres and glass fibres. *Compos Sci Technol*; 62(14):1857–68. [CrossRef]

[20] Rao KMM, Rao KM, Prasad AVR (2010). Fabrication and testing of natural fibre composites: Vakka, sisal, bamboo and banana. *Mater Des*; 31(1):508–13. [CrossRef]

[21] Preethi P, Balakrishna MG (2013). Physical and

Chemical Properties of Banana Fibre Extracted from Commercial Banana Cultivars Grown in Tamilnadu State. *Agrotechnology*; S11:008. [CrossRef]

[22] Ortega Z, Morón M, Monzón MD, Badalló P, Paz R (2016). Production of banana fiber yarns for technical textile reinforced composites. *Materials (Basel)*; 9(5):370. [CrossRef] [PubMed]

[23] Patra AK, Meena LN (2013). Banana fibre in textiles. *Asian Dyer*;10(6):55–59.

[24] Sinha MK (1974). Rope-making with banana-plant fibre. *J Textile Institute*; 65(11):612–615. [CrossRef]

[25] Vigneswaran C, Pavithra V, Gayathri V, Mythili K (2015). Banana Fiber: Scope and Value Added Product Development. *J Text Appar Technol Managem*; 9(2):1-7.

[26] Sumita Y, Honda MJ, Ohara T, Tsuchiya S, Sagara H, Kagami H, *et al* (2006). Performance of collagen sponge as a 3-D scaffold for tooth-tissue engineering. *Biomaterials*; 27(17):3238-48. [CrossRef] [PubMed]

[27] Nugraha B (2017). CelluSponge™ and Go Matrix as innovative three-dimensional cell culture platforms. In Przyborski S (Ed.); *Technology Platforms for 3D Cell Culture: A User's Guide*. John Wiley& Sons.

[28] Cornelissen CG, Dietrich M, Gromann K, Frese J, Krueger S, *et al* (2013). Fibronectin coating of oxygenator membranes enhances endothelial cell attachment. *Biomed Eng Online*; 12:7. [CrossRef] [PubMed]

[29] Pereira ALS, do Nascimento DM, Souza M de SM, Cassales AR, Saraiva Morais JP, *et al* (2014). Banana (*Musa* sp. cv. Pacovan) pseudostem fibers are composed of varying lignocellulosic composition throughout the diameter. *BioResources*; 9(4):7749–63.

[30] Shantha HS, Siddappa GS (1970). Accumulation of Starch in Banana Pseudostem and Fruit. *J Food Sci*; 35(1):74–77. [CrossRef]

[31] Shantha HS, Siddappa GS (1970). Physicochemical nature of banana pseudostem starch. *J Food Sci*; 35(1)72-74. [CrossRef]

[32] Emaga TH, Robert C, Ronkart SN, Wathelet B, Paquot M (2008). Dietary fibre components and pectin chemical features of peels during ripening in banana and plantain varieties. *Bioresour Technol*; 99(10):4346–54. [CrossRef] [PubMed]

[33] Kaviya S, Santhanalakshmi J, Viswanathan B, Muthumary J, Srinivasan K (2011). Biosynthesis of silver nanoparticles using *Citrus sinensis* peel extract and its antibacterial activity. *Spectrochim Acta A Mol Biomol Spectrosc*; 79(3):594–598. [CrossRef]

[34] Jayaprabha JS, Brahmakumar M, Manilal VB (2011). Banana Pseudostem Characterization and Its Fiber Property Evaluation on Physical and Bioextraction. *J Nat Fibers*; 8(3):149–160. [CrossRef]

[35] Sakthivel M, Ramesh S (2013). Mechanical Properties of Natural Fibre (Banana, Coir, Sisal) Polymer Composites. *Sci Park*; 1(1):1-6.

[36] Dhivya S, Keshav Narayan A, Logith Kumar R, Viji Chandran S, Vairamani M, Selvamurugan N (2018). Proliferation and differentiation of mesenchymal stem cells on scaffolds containing chitosan, calcium polyphosphate and pigeonite for bone tissue engineering. *Cell Prolif*; 51(1):e12408. [CrossRef] [PubMed]

[37] Timung R, Deshavath NN, Goud VV, Dasu VV (2016). Effect of Subsequent Dilute Acid and Enzymatic Hydrolysis on Reducing Sugar Production from Sugarcane Bagasse and Spent Citronella Biomass. *J Energy*; 2016:8506214. [CrossRef]

[38] Christopher M, Anusree M, Mathew AK, Nampoothiri KM, Sukumaran RK, Pandey A (2016). Detoxification of acidic biorefinery waste liquor for production of high value amino acid. *Bioresour Technol*; 213:270-275. [CrossRef] [PubMed]

[39] Baharvand H, Hashemi SM, Ashtiani SK, Farrokhi A (2006). Differentiation of human embryonic stem cells into hepatocytes in 2D and 3D culture systems in vitro. *Int J Dev Biol*; 50(7):645-52. [CrossRef] [PubMed]

[40] Zeilinger K, Freyer N, Damm G, Seehofer D, Knöspel F (2016). Cell sources for in vitro human liver cell culture models. *Exp Biol Med (Maywood)*; 241(15):1684-98. [CrossRef] [PubMed]

[41] Lee KD, Kuo TKC, Whang-Peng J, Chung YF, Lin CT, Chou SH, *et al* (2004). In vitro hepatic differentiation of human mesenchymal stem cells. *Hepatology*; 40(6):1275-84. [CrossRef] [PubMed]

[42] Gilbert TW, Freund JM, Badylak SF (2009). Quantification of DNA in Biologic Scaffold Materials. *J Surg Res*; 152(1):135-9. [CrossRef] [PubMed]

[43] Adamski M, Fontana G, Gershlak JR, Gaudette GR, Le HD, Murphy WL (2018). Two methods for decellularization of plant tissues for tissue engineering applications. *J Vis Exp*; 135:57586. [CrossRef] [PubMed]

[44] Maitra A, Murakata LA, Albores-Saavedra J (2001).

Immunoreactivity for hepatocyte paraffin 1 antibody in hepatoid adenocarcinomas of the gastrointestinal tract. *Am J Clin Pathol*; 115(5):689-94. [CrossRef] [PubMed]

[45] Seefeld K, Linder E (2007). Statistics Using R with Biological Examples. CRAN-R Project: https://cran.r-project.org/doc/contrib/Seefeld_StatsRBio.pdf

[46] Wang L, Sun B, Ziemer KS, Barabino GA, Carrier RL (2010). Chemical and physical modifications to poly(dimethylsiloxane) surfaces affect adhesion of Caco-2 cells. *J Biomed Mater Res A*; 93(4):1260-71. [CrossRef] [PubMed]

[47] Gharibzahedi SMT, Jafari SM (2017). The importance of minerals in human nutrition: Bioavailability, food fortification, processing effects and nanoencapsulation. *Trends Food Sci Technol*; 62:119-132. [CrossRef]

[48] Tharmalingam S, Daulat AM, Antflick JE, Ahmed SM, Nemeth EF, Angers S, *et al* (2011). Calcium-sensing receptor modulates cell adhesion and migration via integrins. *J Biol Chem*; 286(47):40922-33. [CrossRef] [PubMed]

[49] Wei C, Wang X, Chen M, Ouyang K, Song LS, Cheng H (2009). Calcium flickers steer cell migration. *Nature*; 457(7231):901-5. [CrossRef] [PubMed]

[50] Ibrahim MM, Dufresne A, El-Zawawy WK, Agblevor FA (2010). Banana fibers and microfibrils as lignocellulosic reinforcements in polymer composites. *Carbohydr Polym*; 81(4):811–819. [CrossRef]

[51] Elanthikkal S, Gopalakrishnapanicker U, Varghese S, Guthrie JT (2010). Cellulose microfibres produced from banana plant wastes: Isolation and characterization. *Carbohydr Polym*; 80(3):852–9. [CrossRef]

[52] Malinen MM, Kanninen LK, Corlu A, Isoniemi HM, Lou YR, Yliperttula ML, *et al* (2014). Differentiation of liver progenitor cell line to functional organotypic cultures in 3D nanofibrillar cellulose and hyaluronan-gelatin hydrogels. *Biomaterials*; 35(19):5110-21. [CrossRef] [PubMed]